Electronic Supplementary Information (ESI) for

Sputtering MoO_2 blocking layer for enhancing the efficiency and dynamic response of CZTSSe solar cells

ShuleiLiang, YingjunZhou, YujunLi, Chuanhe Ma*, and Hailong Wang*

School of Physics and Physical Engineering, Qufu Normal University, Qufu 273165, China

**** Corresponding author;*** *E-mail: machuanhe@126.com, hlwang@qfnu.edu.cn*

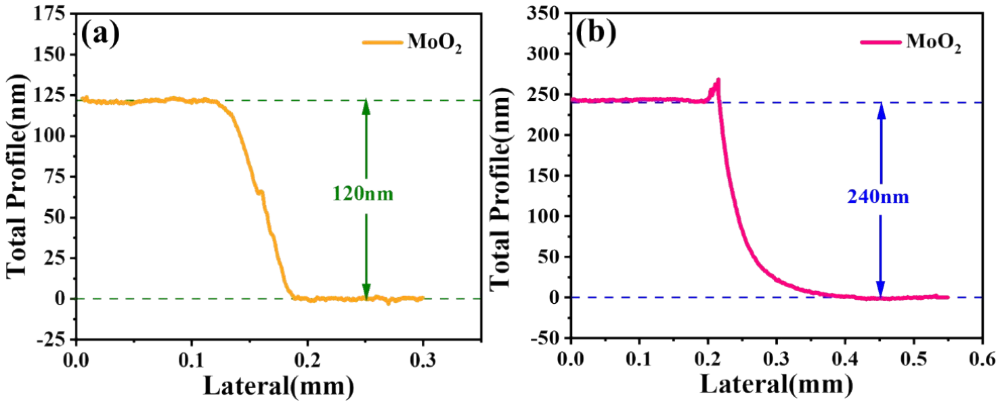

Fig.S1. *Profilometer measurement of MoO_2 films with two sputtering times: (a) 2 hours; (b) 4 hours*

To ensure precise thickness control of sputtered MoO_2 films, optimizing the sputtering parameters is critical. A common lab method involves sputtering thicker films to explore these parameters. Under room temperature, 0.38 Pa argon atmosphere, and 120 W RF power, MoO_2 was sputtered for 2 hours and 4 hours, respectively. The thicknesses measured by the stylus profiler are 120 nm and 240 nm (as shown in Fig.S1(a) and (b)), with clear step edges.This results in a deposition rate of 1 nm/min under these parameters, providing strong data support for subsequent exploration of optimal thickness for blocking layer.

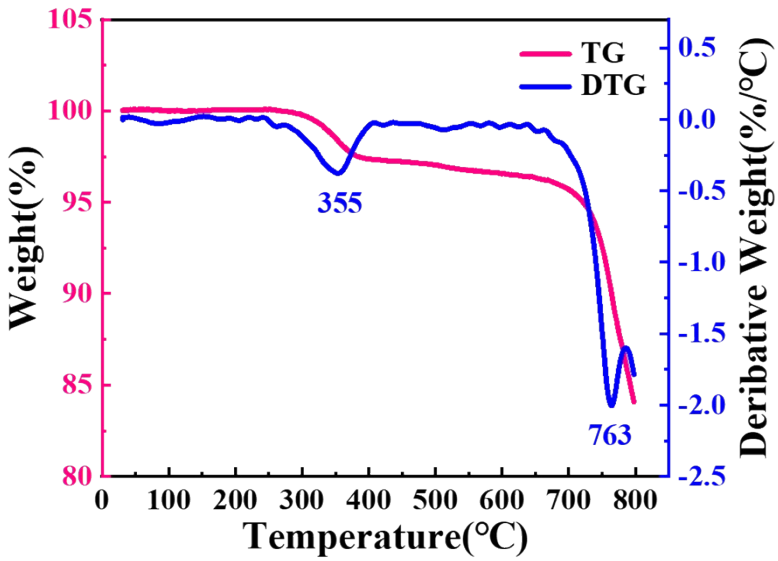

Fig. S2.*The TG and DTG curves of CZTSSe powder*

To study the thermal stability of the absorber layer film, we prepared SLG\CZTSSe sample and scraped off powder to characterize its TG and DTG properties. As shown in Fig. S2, the CZTSSe powder exhibited an initial weight loss of approximately 3% at around 355°C. This may be attributed to the volatilization of excess sulfur atoms (sulfur interstitials, S_i) in kesterite (chemical formula $Cu_2ZnSn(S,Se)_4$) under low saturated vapor pressure. This is contrary to the high-temperature or high vapor pressure conditions (which suppress sulfur volatilization) used in the preparation of $Cu_2ZnSn(S,Se)_4$. Under low saturated vapor pressure conditions, sulfur atoms are more likely to escape from the lattice (volatilization), leading to the formation of sulfur vacancy defects. In the temperature range of 380-700°C, the weight loss of the CZTSSe powder was relatively slow, corresponding to the decomposition reaction and volatilization of sulfur (selenium) molecules as described by Equation (I). In the range of 700-800°C, the CZTSSe powder experienced a sharp weight loss, at which point SnS(Se) also began to volatilize[1].

$$2Cu_2ZnSn(S,Se)_4 \rightarrow 2Cu_2S(Se)+2ZnS(Se)+2SnS(Se)+S(Se)_2 \quad (I)$$

The above TG and DTG tests indicate: (1) The adsorption of sulfur (selenium) molecules and the formation of polycrystalline in the CZTSSe absorber layer begin at approximately 355°C; (2) during the sputtering of the window layer (ZnO and ITO) or overall device air-annealing, a substrate temperature can be applied, but it should not exceed 300°C, otherwise it will lead to sulfur element volatilization and an increase in the back interface $Mo(S,Se)_2$ layer thickness.

Although the powder scraped from the SLG\CZTSSe sample does not fully represent a reliable thermogravimetric measurement of the entire CZTSSe device due to practical

limitations, the thermal decomposition behavior observed in the powder still provides important insights into the stability of the CZTSSe material system. The volatilization of sulfur species and decomposition reactions identified through powder analysis are intrinsic characteristics of the CZTSSe compound, and under similar thermal conditions, these processes can reasonably be expected to occur in the thin-film form as well. We will also explicitly connect these findings to device processing considerations, particularly regarding the maximum allowable temperature (<300°C) during window layer (ZnO and ITO) sputtering or overall device air-annealing, to prevent sulfur loss and excessive $Mo(S,Se)_2$ formation at the back contact, which directly impacts device performance and long-term stability.

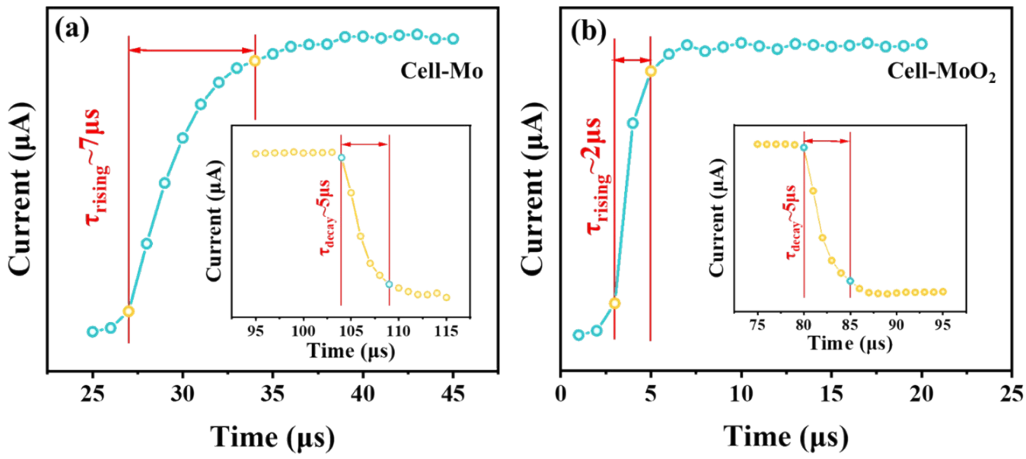

Fig. S3. *I-T curves of the rising edge and falling edge for the two devices under 10 kHz, 70% duty cycle laser pulse excitation: (a) Cell-Mo; (b) Cell-MoO_2*

As shown in Fig. S3, the time response characteristics of the two devices are described. The pulse rise time (τ_{rising}) of Cell-MoO_2 is 2 μs, much lower than that of Cell-Mo (7 μs), indicating its faster capture of optical signal changes. The pulse fall time (τ_{decay}) of both devices is 5 μs, suggesting comparable performance during signal decay.

The difference in light response capability indicates that the Cell-MoO_2 device may have superior carrier mobility, enabling rapid accumulation of photogenerated carriers under pulse excitation and thus enhancing the peak photocurrent. The short τ_{rising} of Cell-MoO_2 is attributed to its fewer interface trap states and higher carrier injection efficiency, while the longer τ_{rising} of Cell-Mo may arise from interface recombination losses [2].

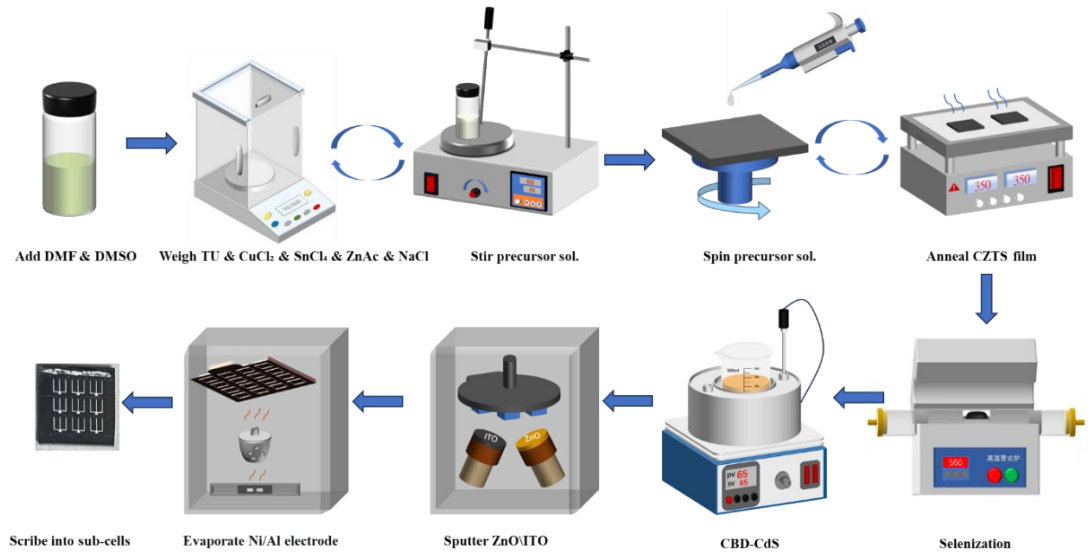

Fig. S4. *Fabrication Process Flow of CZTSSe Solar Cells*

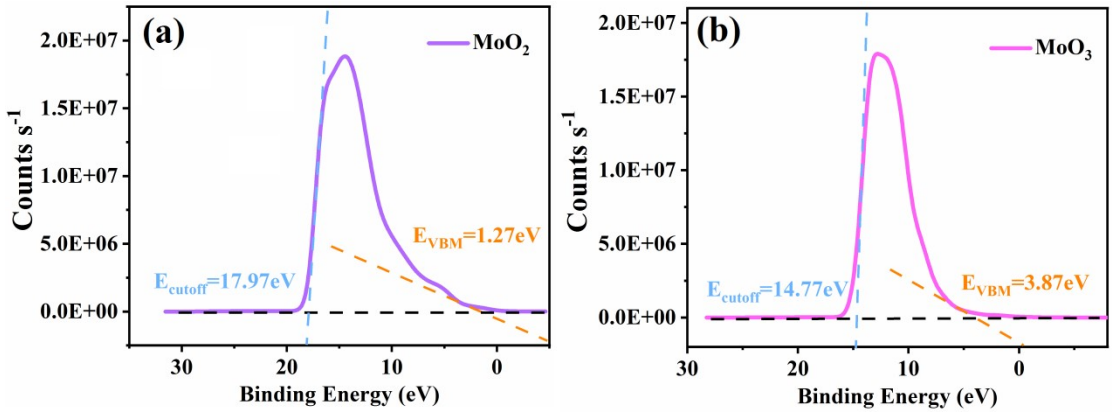

Fig. S5. *UPS fitting plots for (a) MoO_2 sample; (b) MoO_3 sample*

Annealing at 350 °C for 10 minutes promotes the oxidation of Mo^{4+} to Mo^{6+} by reducing oxygen vacancies ($O_{vac.}$) and increasing lattice oxygen ($O_{lat.}$) content, which could indeed significantly affect the surface electronic structure and band alignment. To verify this hypothesis, we performed UPS measurements on the MoO_2 sample (structure: SLG\Mo\$MoO_2$) and the MoO_2 sample (structure: SLG\Mo\$MoO_2$).

UPS measurements were performed on an ESCALAB 250Xi X-ray photoelectron spectrometer equipped with a He discharge lamp. The typical base pressure in the spectrometer chamber was 2×10^{-10} Pa. The UPS spectra were recorded using unfiltered He I (21.22 eV) excitation, with a bias of −5.00 V applied to the samples to observe the low-energy secondary electron cutoff. The UV spot size on the samples was approximately 600

μm in diameter. The typical instrument resolution for UPS measurements was 0.05 eV, with a photon energy dispersion of less than 20 meV.

As shown in Fig. S5, the cutoff binding energy measured on the MoO_2 surface is 17.97 eV, from which the work function is derived to be 3.25 eV by subtracting the photon energy of 21.22 eV. For the MoO_2 film, E_f–E_{VBM}=1.27 eV, where E_f is the Fermi level and E_{VBM} is the valence band maximum. For the MoO_3 surface, the measured cutoff binding energy is 14.77 eV, yielding a work function of 6.45 eV after subtracting the photon energy of 21.22 eV. The E_f–E_{VBM} value for the MoO_3 film is 3.87 eV. Based on these data, the ionization potentials (IP) of the MoO_2 and MoO_3 films are calculated to be 4.52 eV and 10.32 eV, respectively. Detailed parameters are provided in Table S1.

MoO_3 exhibits a high work function (6.45 eV), characteristic of a typical wide-bandgap n-type oxide semiconductor. MoO_2 has a low work function (3.25 eV), suggesting it behaves as a metallic-like narrow-bandgap n-type oxide semiconductor [3]. However, it should be noted that in the MoO_2 sample (structure: SLG\Mo\$MoO_2$) and the MoO_3 sample (structure: SLG\Mo\$MoO_3$), the MoO_2 and MoO_3 blocking layers serve as a sacrificial barrier. Specifically, during high-temperature selenization annealing at 560 °C, both MoO_2 and MoO_3 disappear (are sacrificed) and transform into $MoSe_2$. After selenization, the absorber layer sample structure becomes SLG\Mo\$MoSe_2$\CZTSSe, and the final device structure is SLG\Mo\$MoSe_2$\CZTSSe\CdS\ZnO\ITO, where no blocking layer (MoO_2 or MoO_3) remains. The purpose of introducing this blocking layer is to suppress the reaction between Mo and Se vapor under low-temperature conditions, thereby reducing the thickness of the $MoSe_2$ layer.

Table S1. *Fitted valence band parameters of MoO_2 and MoO_3 samples, where $E_{cutoff,\,B.E.}$ (eV) is the binding energy of the secondary electron cutoff, hν is the excited He I spectral line, Φ represents the work function, E_f is the Fermi level, E_{VBM} is the valence band maximum energy, IP represents the ionization potential (E_{vac}–E_{VBM}), and E_{vac} represents the vacuum level.*

Sample	**$E_{cutoff,B.E.}$ (eV)**	**hν (eV）**	**Φ (eV)**	**E_f-E_{VBM} (eV)**	**IP (eV)**
MoO_2	17.97	21.22	3.25	1.27	4.52
MoO_3	14.77	21.22	6.45	3.87	10.32

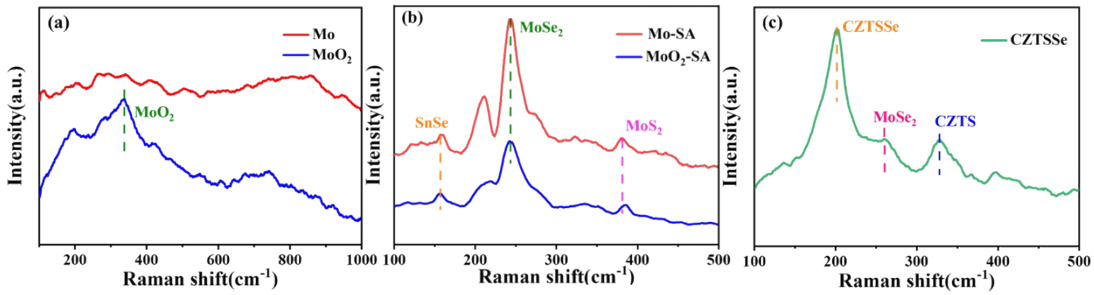

Fig.S6. *Raman spectra of (a) Mo and MoO_2 samples; (b) Mo-SA and MoO_2-SA samples after selenization annealing; (c) CZTSSe absorber samples.*

To verify that the introduction of a MoO_2 blocking layer can effectively suppress the formation of $MoSe_2$, Raman spectroscopy was performed on commercial Mo-coated glass (SLG\Mo) and a sample with an additional sputtered MoO_2 layer (SLG\Mo\200nm MoO_2). As shown in Fig. S6(a), the commercial Mo substrate shows no obvious Raman features. In contrast, the prepared MoO_2 sample exhibits a prominent peak at 326 cm^{-1}, characteristic of MoO_2, confirming the successful preparation of the designed blocking layer.

The Mo and MoO_2 samples were converted into Mo-SA and MoO_2-SA samples, respectively, after selenization annealing. As shown in Fig. S6(b), both the Mo-SA and MoO_2-SA samples exhibit peaks corresponding to $MoSe_2$ (250 cm^{-1}), MoS2 (383 cm^{-1}), and SnSe (156 cm^{-1}). These peaks originate from chemical reactions between the Mo-based layers and the Se and S vapors generated from the Se and SnS powders added into the graphite box at high temperatures. A detailed comparison reveals that the intensity of the $MoSe_2$ peak for the MoO_2-SA sample is significantly lower than that for the Mo-SA sample, indicating that the MoO_2 layer effectively suppresses the formation of $MoSe_2$.

We scratched off a portion of the absorber film (SLG\Mo\$MoSe_2$\CZTSSe), formed by selenizing a precursor with the structure SLG\Mo\10nm MoO_2\CZTS, for Raman measurement. Apart from the CZTSSe peak (196 cm^{-1}), $MoSe_2$ peak (250 cm^{-1}), and CZTS peak (338 cm^{-1}), no MoO_2 Raman peak was detected. Conversely, as shown in Fig. 9(d), the chemically formed $MoSe_2$ layer at the back interface of Cell-MoO_2 has a thickness of 300 nm. This further confirms that at a high temperature of 560 °C, the 10 nm MoO_2 layer completely reacts with Se and transforms into $MoSe_2$, indicating the absence of MoO_2 in the back interface structure of Cell-MoO_2. Consequently, the back interface structures (band-alignment structures) of both Cell-Mo and Cell-MoO_2 are SLG\Mo\$MoSe_2$\CZTSSe, with the distinction that the Cell-MoO_2 back interface achieves a relatively thinner $MoSe_2$ layer (300 nm) through the consumption of the MoO_2 layer.

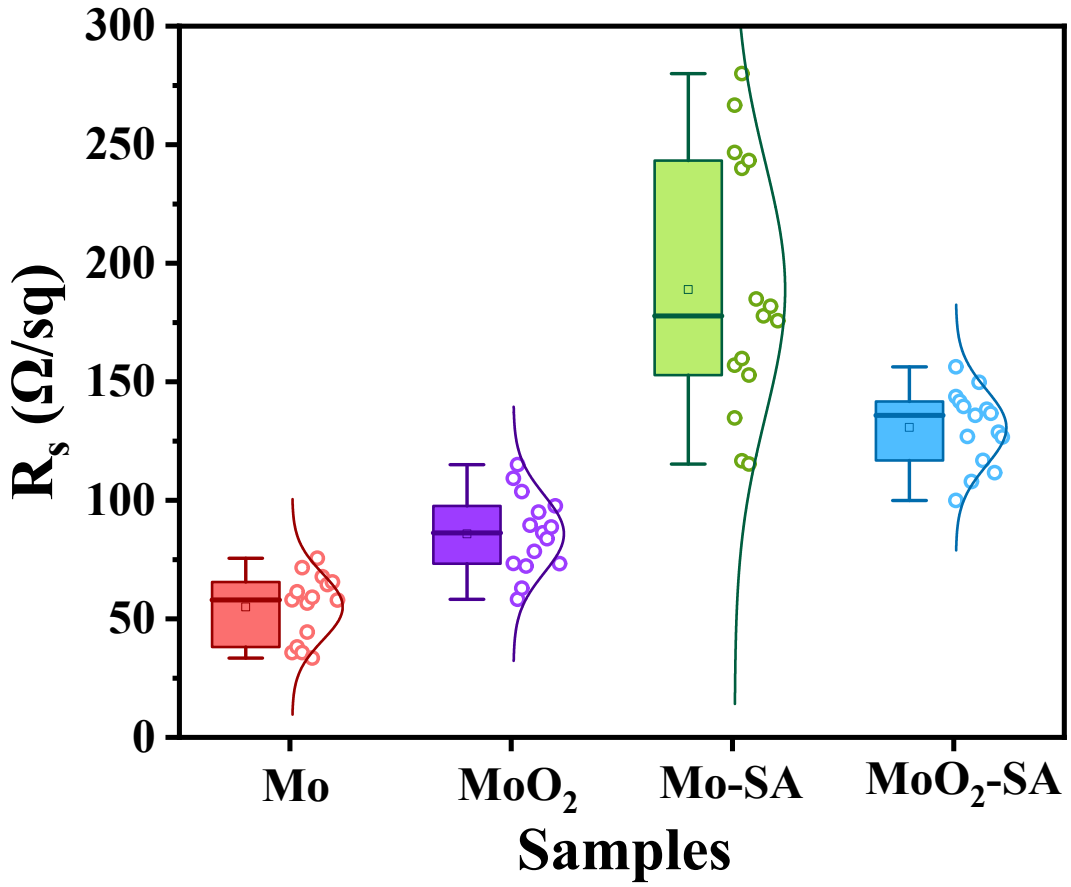

Fig. S7. *Sheet resistance statistics of Mo, MoO_2, Mo-SA, and MoO_2-SA samples, with 15 devices per condition and 50 devices total, to validate reproducibility.*

To investigate the effect of the MoO_2 blocking layer on electrical performance, we measured the sheet resistance of as-deposited Mo and MoO_2 samples prior to selenization. As shown in Fig. S7, the statistics are based on 15 samples per condition. The pristine Mo samples exhibited a sheet resistance of 55 ± 14 Ω, while the MoO_2-coated samples showed a higher average value of 86 ± 16 Ω. The relatively low standard deviations indicate good film uniformity for both types of samples.

The significant reduction in sheet resistance from 189 ± 54 Ω for the Mo-SA sample to 131 ± 16 Ω for the MoO_2-SA sample after selenization can be attributed to the controlled growth of the $MoSe_2$ interlayer. The MoO_2 layer acts as a sacrificial barrier, limiting the reaction with Se vapor and resulting in a thinner and more uniform $MoSe_2$ layer compared to the thick, irregular $MoSe_2$ formed on the bare Mo substrate. The reduced standard deviation further confirms the enhanced uniformity and reproducibility of the back contact achieved with the MoO_2 blocking layer. This improvement is crucial for reducing the series resistance in complete devices, thereby potentially enhancing the short-circuit current density, fill factor, and overall performance of CZTSSe solar cells.

Notes and references

(1) A. Redinger, D. M. Berg, P. J. Dale and S. Siebentritt, *J. Am. Chem. Soc.,* 2011, **133**, 3320–3323.

(2) H. Wu, C. Ma, J. Zhang, H. Cao, R. Lin, W. Bai, Z. Pan, J. Yang, Y. Zhang, Y. Chen, X. Tang, X. Wang, J. Wang and J. Chu, *ACS Appl. Electron. Mater.,* 2021, **3**, 4135–4143.

(3) Irfan, F. So and Y. Gao, *International Journal of Photoenergy,* 2011, **2011**, Article ID 314702, 1-6.